Tuning the group delay of optical wave packets in liquid-crystal light valves

U. Bortolozzo,[1] S. Residori,[1] and J. P. Huignard[2]
[1]*Institut Non Linéaire de Nice, 1361 Route des Lucioles, 06560 Valbonne-Sophia Antipolis, France*
[2]*Thales Research and Technology, RD 128, 91767 Palaiseau Cedex, France*
(Received 1 September 2008; published 18 May 2009)

By performing two-wave mixing experiments in a liquid-crystal light valve, optical pulses are slowed down to group velocities as slow as a few tenths of mm/s, corresponding to a very large group index. We present experiments and model of the slow-light process occurring in the liquid-crystal light valve, showing that this is characterized by multiple-beam diffraction in the Raman-Nath regime. Depending on the initial frequency detuning between pump and signal, the different output order beams are distinguished by different group delays. The group delay can be tuned by changing the main parameters of the experiment: the detuning between the pump and the input wave packet, the strength of the nonlinearity, and the intensity of the pump beam.

DOI: 10.1103/PhysRevA.79.053835 PACS number(s): 42.65.Hw, 42.50.Gy, 42.70.Df, 77.22.Gm

I. INTRODUCTION

The ability to control the group delay of light pulses has recently received a large interest, and slow- and fast-light phenomena have been observed in different systems [1]. The possibility to obtain slow light has recently been identified as a solution to the problem of pulse buffering in optical communication systems [2]. In addition, it has been pointed out that slowing down optical pulses can be used to enhance the spectral sensitivity of certain types of interferometers [3], which is expected to have a significant impact in applications such as precision metrology and optical sensing. Moreover, fast light has been proposed as a method to enhance the sensitivity of gravitational wave detectors, which has been tested either by employing bifrequency Raman gain in atomic vapors [4] or double pumped two-wave mixing (TWM) in photorefractive crystals [5].

Much of the early research into slow light was carried out using electromagnetically induced transparency in atomic vapors [6] or ultracold atoms [7]. More recently, a considerable deceleration of light pulses was obtained in room temperature solids, such as ruby crystals, through the quantum coherence effect [8], and in photorefractive crystals through the strong dispersion of dynamic gratings in the vicinity of Bragg resonance [9–11]. Based on the finite material response time, slow- and fast-light effects have also been predicted in Kerr media without a pump [12].

Recently, we have shown that slow- and indeed fast- light phenomena are possible using liquid-crystal (LC) light valves [13]. Liquid crystal light valves offer the potential for slowing whole images, a slow-light feature recently demonstrated in atomic vapor experiments [14], and possess unique features for practical implementations, such as a large electro-optic response, visible and near ir transparency, small-size operating devices, and widespread technological impact. Slow- and fast-light phenomena were obtained in a liquid-crystal light valve (LCLV) by performing nondegenerate TWM experiments and by exploiting the dispersion properties associated with the gain features of the mixing process. The LCLV is made by the association of a nematic liquid-crystal layer and a photorefractive crystal [15] and has recently been demonstrated as an attractive and versatile medium for nonlinear optics [16] and beam-coupling experiments [17]. In TWM experiments the LCLV operates in the Raman-Nath regime of diffraction [18], thus several output orders are observed at the exit of the cell. Depending on the diffraction order considered and on the initial frequency detuning between pump and signal, different group delays are obtained in a single experiment, with the output pulse either anticipated or delayed.

Here, we present a theoretical model of the slow- and fast-light processes occurring in LCLVs through the nonlinear wave mixing in the Raman-Nath regime of diffraction. The model accounts for the different group delays observed on the different output order beams, thus allowing calculating the group velocity for each order output. The theoretical predictions are compared with the experimental results, showing good agreement.

The paper is organized as follows. In Sec. II, we describe the LCLV and its working characteristics. In Sec. III we introduce the equations for the beam-coupling in thin media and in Sec. IV we present the theory of slow- and fast-light phenomena through the nonlinear wave mixing in the Raman-Nath regime. In Sec. V, we report the experimental data and the comparison with the theoretical predictions. In Sec. VI, we discuss the dependence of the group velocity on the different experimental parameters. Finally, Sec. VII presents the conclusions.

II. LIQUID CRYSTAL LIGHT VALVE

As schematically represented in Fig. 1, the liquid-crystal light valve is formed by the association of a LC layer with the inorganic crystal $Bi_{12}SiO_{20}$ (bismuth silicate, usually abbreviated as BSO), cut in the form of a cell wall, 1 mm thickness, 20×30 mm^2 lateral size. The other wall is a glass (BK7) window. The BSO is well known for its photorefractive properties and here is used for its large photoconductivity and transparency in the visible range [19]. While the BSO acts as a photoconductor, the electro-optic effect is provided by the large birefringence of the LC layer.

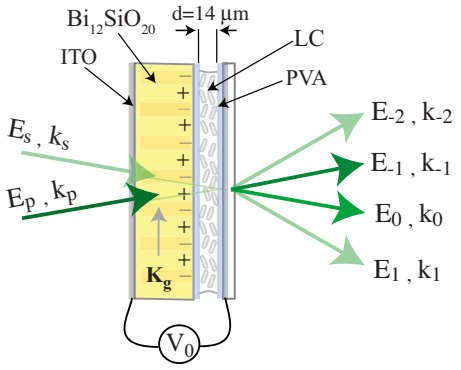

FIG. 1. (Color online) Schematic representations of the liquid-crystal light valve and of the two-beam coupling occurring in the liquid-crystal layer.

Liquid crystals are strongly anisotropic materials composed of elongated organic molecules. Their main feature is that it exists a temperature range in within they constitute mesophases, that is, they form phases with properties intermediate between solids and liquids [20]. The nematic phase is characterized by a long range orientational order, for which all the molecules are in average aligned along a preferential direction, so called the nematic "director." Since the liquid-crystal molecules have a different polarizability along their long and short axes, a nematic layer as a whole behaves like a strongly birefringent material, characterized by an extraordinary and an ordinary refractive index with typical values of $n_e=1.7$ and $n_0=1.5$, respectively.

When placed into contact with surfaces, liquid crystals spontaneously assume orientations that depend sensitively on the topography and chemical functionality of the surfaces. In order to obtain an ordered nematic layer, the surfaces of the confining walls have to be specifically treated with products able to impose a strong anchoring at the boundaries, either through electrostatic forces or through mechanical rubbing [21]. For this purpose, before assembling the light valve both the surfaces of the BSO and of the glass window that will be in contact with the liquid crystals are coated with polyvinyl alcohol (PVA), which is then polymerized and rubbed to obtain planar alignment of the liquid crystals (nematic director parallel to the confining walls). After this treatment, Teflon spacers of $d=14$ μm are inserted between the two walls; the gap is filled with the liquid crystal and then is sealed with uv photopolymerizing glue.

Under the application of an electric voltage, LC tends to align along the direction of the applied field, and, because of the birefringence, the refractive index changes accordingly, which is the mechanism at the basis of commercial liquid-crystal displays [22]. In the light valve, to allow the application of an external voltage V_0 the outside surface of the BSO and the inside of the glass window (before the PVA layer) are coated with an indium-tin-oxide (ITO) transparent electrode. The typical voltage applied is ac, with a rms value from 2 to 20 V and a frequency from 50 Hz to 20 kHz. Since the BSO modulates the effective voltage across the LC as a function of the incident light intensity, in the light valve the LC orientation and thus the refractive index depend on the local illumination on the photoconductive layer [15].

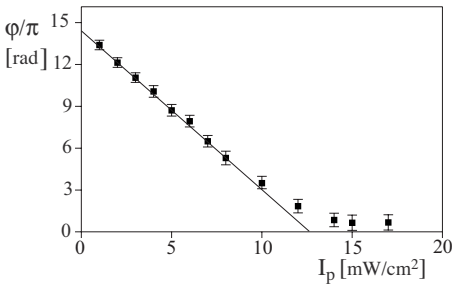

FIG. 2. Phase retardation provided by the light valve as a function of the pump intensity I_p; the applied voltage is fixed to $V_0=22$ V_{rms} and frequency $f=1$ kHz.

The LC reorientation process requires the collective motion of the molecules to establish over the whole thickness d of the nematic layer. Therefore, the LC response time is given by

$$\tau_{LC} = \gamma d^2/K, \tag{1}$$

where γ is the LC rotational viscosity and K is the splay elastic constant [20] and is on the order of 100 ms for $d=14$ μm and typical values of the LC constants. Note that, due to the slow relaxation time, the LC molecules cannot follow the oscillation of the ac applied field. Instead, they perform a static reorientation, in which they reach an equilibrium position fixed by the rms value of the applied field. The reason for applying an ac field is that the complex impedances of the photoconductive and LC layers require an optimal frequency range in order to achieve a good contrast of the LC voltage with and without illumination [15].

A typical response of the LCLV is displayed in Fig. 2. It was obtained by sending onto the valve an enlarged and collimated laser beam, waist of 18 mm, $\lambda=532$ nm, and by recording the fringe displacement in an interferometric setup, where the output beam is made to interfere with a reference beam. The phase retardation φ experienced by the beam that has passed through the light valve is plotted in Fig. 2 as a function of the input intensity I_p. The saturation of the response is attained when the liquid crystals are aligned along the direction of the applied field. The full range of phase variation is $\varphi \sim 12\pi$, which corresponds to the maximum birefringence $\Delta n=n_e-n_o=0.2$ of the LC layer. In the linear part of the response ($I_p<5$ mW/cm^2) the LCLV behaves as a Kerr-type nonlinear medium, with a refractive index change $\Delta n \propto I_p$ and a typical response time of about 100 ms.

While in conventional reflective-type light valves [23] beam-coupling experiments were forbidden by the optical isolation between the input and readout beams, the transmissive configuration of the photorefractive LCLV can be largely exploited for performing wave mixing experiments [17]. In the LCLV the beam coupling takes place over a large working area and extra optical and electric control can be achieved through the addressing of the photoconductive BSO layer. In the past, wave mixing phenomena have been extensively studied in photorefractive materials, leading to a large number of attractive effects, such as real-time holography and dynamic gratings [24], sensitivity enhanced interferometry [25], light induced waveguides [26], and spatial solitons

[27]. Similar mechanisms are also at the base of the gain process and transverse spatiotemporal dynamics in photorefractive cavities [28–30].

Now that beam-coupling experiments can be implemented in the LCLV, new performances are expected, which are related to the specific features of the LC layer, for example, the large birefringence and the possibility of operating over thin active layers, eventually in multipassage or cascaded configurations [31]. Here, we will focus our attention on the possibility of using two-wave mixing to obtain slow- and fast-light phenomena by exploiting the large dispersive properties associated to the gain features of the mixing process.

III. TWO-BEAM COUPLING IN THE LCLV

Two-wave mixing experiments are performed by following the scheme shown in Fig. 1. A signal beam, E_s, is sent to the LCLV together with a pump beam, E_p. The ratio between the pump and signal intensities is defined as $\beta \equiv I_p/I_s$, with $I_p=|E_p|^2$ ad $I_s=|E_s|^2$, and is a parameter of the experiment. Usually, β is much larger than 1, so that the pump beam is at much higher intensity of the signal beam. The two beams are enlarged and collimated, waist 18 mm, and interfere in the plane of the BSO giving rise to an intensity fringe pattern. In the experiment, the fringe spacing is usually varied from 100 to 300 μm, which corresponds to an interference angle θ from 27 to 0.9 mrad.

For these small values of the interference angle, the superposition region, within which the interference fringes are the same, extends in the longitudinal direction over several millimeters. Therefore, the fringe pattern is the same on the whole BSO body, comprised its outer and inner surfaces. In correspondence, the photoconductive response of the BSO leads to a photoinduced space charge distribution that induces a spatially periodic reorientation of the liquid-crystal molecules. Due to the LC birefringence, a refractive index grating is thus formed inside the liquid-crystal layer.

The two writing beams are diffracted by the same grating they are inducing in the LC layer. Since the liquid-crystal layer is thin with respect to the fringe spacing, the beam coupling occurs in the Raman-Nath regime of diffraction and several diffracted beams are observed at the output of the light valve. This situation is different from the TWM occurring in the Bragg regime. Indeed, it is known from Kogelnik's coupled wave theory [32] that, when the two-wave mixing occurs in thick media, constructive interference between the diffracted pump and signal can only take place in one direction, which is the one satisfying the Bragg condition. In the Raman-Nath regime, we observe multiple diffracted orders distinguished by the numbers $0, \pm 1, \pm 2, \ldots, \pm m$. Due to the self-diffraction and beam-coupling phenomena, the pump is transferred into the $m=0,+1,\ldots$ orders, which receive gain, i.e., they receive more photons than they are losing. The $m=-1$ order is the pump beam that, even though depleted, remains of much higher intensity than the other beams [31].

More precisely, the total electric field arriving on the BSO side of the LCLV can be written as

$$E_{in}(\vec{r},t) = E_s e^{i[\vec{k}_s\cdot\vec{r}-\omega_s t]} + E_p e^{i[\vec{k}_p\cdot\vec{r}-\omega_p t]} + \text{c.c.}, \tag{2}$$

with E_s and E_p as the signal and the pump beam, respectively, with wave vectors $\vec{k}_s$, $\vec{k}_p$ and frequencies ω_s, ω_p. The frequency detuning between pump and signal is denoted as

$$\delta = \omega_p - \omega_s. \tag{3}$$

The two beams give rise to an intensity fringe pattern,

$$\begin{aligned} |E_{in}(\vec{r},t)|^2 &= |E_s|^2 + |E_p|^2 + 2E_pE_s\cos(\vec{K}_g\cdot\vec{r}-\delta t) \\ &= I_{in}\left[1 + 2\frac{E_pE_s}{I_{in}}\cos(\vec{K}_g\cdot\vec{r}-\delta t)\right], \end{aligned} \tag{4}$$

where $I_{in} \equiv |E_s|^2+|E_p|^2=I_s+I_p$ is the total input intensity and

$$\vec{K}_g = \vec{k}_p - \vec{k}_s \tag{5}$$

is the grating wave vector. Through the photoconductive effect, the fringe pattern induces, on its turn, a molecular reorientation pattern in the liquid-crystal layer, hence a refractive index grating with the same wave vector K_g and spatial period $\Lambda \equiv 2\pi/K_g$.

The amplitude $n(\vec{r},t)$ of the refractive index grating is governed by a Debye relaxation equation [20],

$$\tau_{\text{LC}}\frac{\partial n}{\partial t} = -(1 - l_d^2\nabla^2)n + n_c + n_2|E_{in}|^2, \tag{6}$$

which follows from the relaxation dynamics of the LC molecules, where τ_{LC} is the LC relaxation time, l_d is the transverse diffusion length due to elastic coupling in the LC and charge diffusion in the photoconductive layer, and n_2 is the equivalent Kerr-type coefficient of the LCLV, the minus sign accounting for the defocusing character of the LCLV nonlinearity [31].

By coupling the above equation [Eq. (6)] with the wave equation for the input electric field,

$$\nabla^2 E - \left(\frac{n}{c}\right)^2\frac{\partial^2 E}{\partial t^2} = 0, \tag{7}$$

with boundary conditions given by Eq. (2), $E=E_{in}$ at $z=0$, we obtain the output diffracted field in the Raman-Nath regime. For the m order of diffraction the output field can be written as

$$\tilde{E}_m = E_m e^{i(\vec{k}_m\cdot\vec{r}-\omega_m t)} + \text{c.c.}, \tag{8}$$

where

$$\omega_m = \omega_s - m\delta \tag{9}$$

is its frequency and

$$\vec{k}_m = \vec{k}_s - m\vec{K}_g \tag{10}$$

is its wave vector. The amplitude is given by

$$E_m = [E_sJ_m(\rho) + iE_pJ_{m+1}(\rho)e^{-i\Psi}]\cdot e^{i[k(n_c+kn_2I_{in})z+m(\pi/2-\Psi)]}, \tag{11}$$

where J_m is the Bessel function of the first kind and of order m,

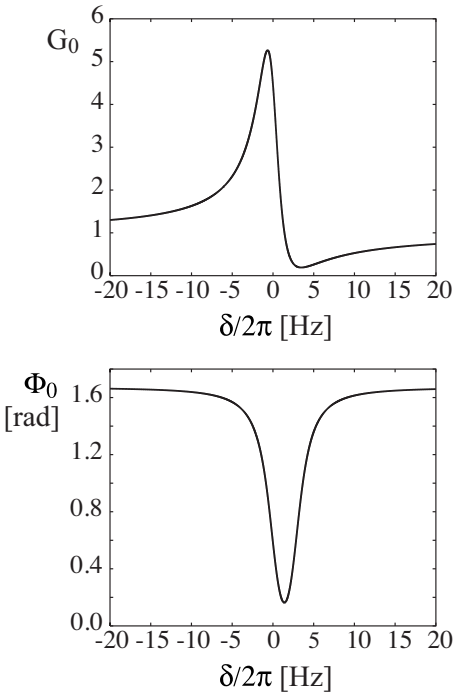

FIG. 3. (a) Gain G_0 and (b) phase shift Φ_0 for the $m=0$ output order beam as a function of the frequency detuning δ between the pump and signal, $\beta=80$.

$$\rho = \frac{2kn_2E_pE_s}{\sqrt{(1+l_d^2K_g^2)^2+(\delta\tau_{\mathrm{LC}})^2}}d, \tag{12}$$

and

$$\tan\Psi = \frac{\delta\tau_{\mathrm{LC}}}{1+l_d^2K_g^2}. \tag{13}$$

From the above equations [Eq. (11)], we can derive the gain G_m and the nonlinear phase shift Φ_m for each output order m. By taking the usual definition for the TWM gain, we can write the gain of the order m as

$$G_m = \frac{|E_m|^2}{I_s}. \tag{14}$$

On the other side, the nonlinear phase shift is given by the phase of the m output order beam, that is,

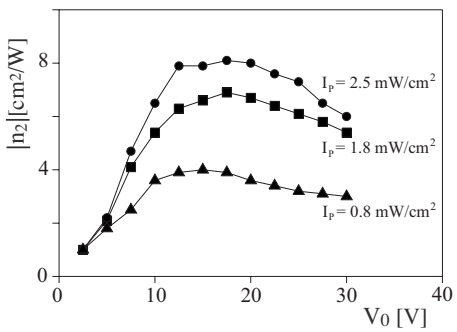

FIG. 4. LCLV nonlinear coefficient n_2 measured as a function of the voltage V_0, $f=1$ kHz, and for different pump intensities.

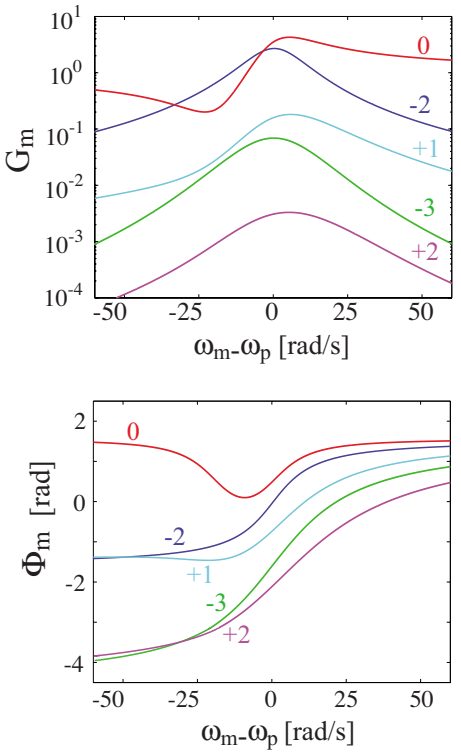

FIG. 5. (Color online) Theoretical variation in (a) gain G_m and (b) phase shift Φ_m as a function of the frequency $(\omega_m-\omega_p)$ of the m order output, $\beta=30$.

$$\tan\Phi_m = \frac{\mathrm{Im}(E_m)}{\mathrm{Re}(E_m)}. \tag{15}$$

If we limit our analysis to the $m=0$ beam that coincides with the original propagation direction of the input signal, we have

$$E_0 = \sqrt{G_0}E_s e^{i\Phi_0}e^{i(\vec{k}_s\cdot\vec{r}-\omega_s t)}. \tag{16}$$

When $\rho \ll 1$ the TWM gain $G_0=|E_0|^2/I_s$ is given by

$$G_0 = 1 + 2g\,\sin(\Psi)z + g^2z^2, \tag{17}$$

where

$$g = \frac{kn_2I_p}{\sqrt{(1+l_d^2K_g^2)^2+(\delta\tau_{\mathrm{LC}})^2}}, \tag{18}$$

and the phase shift is given by

$$\Phi_0 = \tan^{-1}\left(\frac{kn_2I_p\cos(\Psi)z}{\sqrt{(1+l_d^2K_g^2)^2+(\delta\tau_{\mathrm{LC}})^2}+kn_2I_p\sin(\Psi)z}\right) + k[n_c+n_2I_{in}]z. \tag{19}$$

G_0 and Φ_0 are plotted in Figs. 3(a) and 3(b), respectively, as a function of the frequency detuning δ. The values of the parameters, chosen by following the typical experimental conditions, are $\tau_{\mathrm{LC}}=120$ ms, $l_d=14$ μm, $\Lambda=250$ μm, $n_2=-6$ cm^2/W, $I_p=2$ mW/cm^2, and $\beta=80$. The maximum gain is obtained for $\delta\sim 0$. Note that for $\delta=0$ and in the limit

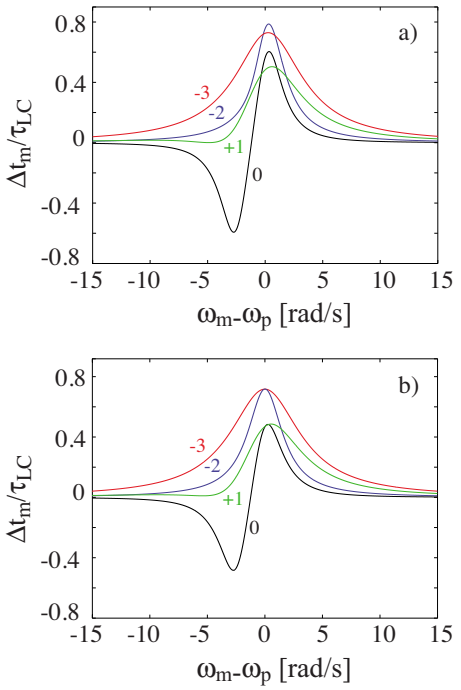

FIG. 6. (Color online) Theoretical variation in the group delay Δt_m as a function of the frequency $(\omega_m - \omega_p)$ of the m order output for (a) $\beta=3$ and (b) $\beta=30$.

$l_d^2 K_g^2 \ll 1$, a condition that is often satisfied in the experiments, the above expression for G_0 [Eq. (17)] reduces to the already known formula [33]

$$G_0 = 1 + (k n_2 I_p)^2 d^2, \tag{20}$$

where $z=d$ is the thickness of the LC layer.

Experimentally, we can measure G_0 as the ratio of the output to the input signal intensity and, by using the above expression [Eq. (20)], we can derive the nonlinear coefficient n_2.

As an example, we report in Fig. 4 the n_2 measured as a function of the voltage V_0 applied to the LCLV and for different pump intensities. In this set of measurements the frequency of the applied voltage was 1 kHz. The large value of n_2 reflects the large and slow nonlinear response of the LCLV. Note that the nonlinear coefficient n_2 is the local slope $\partial n/\partial I$ of the LCLV response; therefore it is not a constant but depends both on the applied voltage and on the pump intensity. Once fixed the pump intensity, the strength of the nonlinearity can be tuned by varying the voltage V_0 applied to the LCLV.

IV. SLOWING DOWN LIGHT PULSES BY THE NONLINEAR WAVE MIXING

We now consider the general case of m output order beams. In Figs. 5(a) and 5(b) we report the theoretical variation in G_m and Φ_m, respectively, as a function of ω_m and for different orders m. The plots in Fig. 5(a) are in log-ln scale and are numerically calculated for $\tau_{LC}=120$ ms, $l_d=14$ μm, $\Lambda=150$ μm, $n_2=-6$ cm^2/W, $I_p=2$ mW/cm^2, and $\beta=30$.

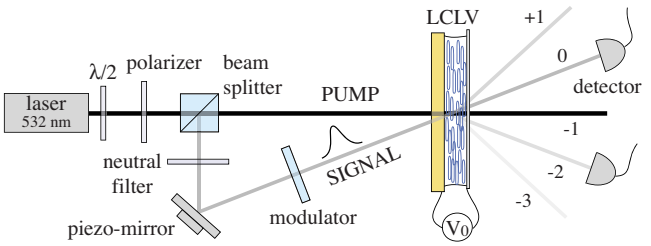

FIG. 7. (Color online) Experimental setup.

The group delay Δt_m of the output order m is given by the slope of the dispersion curve,

$$\Delta t_m = \frac{\partial \Phi_m}{\partial \omega_m}, \tag{21}$$

and the group velocity of each pulse can thus be calculated as

$$v_m \equiv \frac{d}{\Delta t^{(m)}}, \tag{22}$$

with d as the thickness of the LC layer. Note that for every m the slope of the Φ_m curves is maximum for $\delta=0$ $(\omega_m=\omega_p)$; hence the maximum group delay is obtained when the pump and signal have the same frequency.

For $\delta=0$ the analytical expression of the maximum group delay for the m output order is

$$\Delta t_m^{(\max)} = \frac{m}{m+1}\tau_g + \frac{1}{m+1}\left[\frac{\beta\left(\frac{J_{m+1}(\rho)}{J_m(\rho)}\right)^2}{1+\beta\left(\frac{J_{m+1}(\rho)}{J_m(\rho)}\right)^2}\right]\tau_g, \tag{23}$$

where

$$\tau_g = \frac{\tau_{LC}}{1 + l_d^2 K_g^2} \tag{24}$$

is the normalized response time of the liquid crystals

$$\tau_g \simeq \tau_{LC} \tag{25}$$

for $l_d^2 K_g^2 \ll 1$.

Theoretically, the maximum group delay is $2\tau_g$ and it is achieved for the $m=-2$ order, whereas for the other orders the maximum group delay is τ_g. Correspondingly, the maximum fractional delays that we can achieve are 1 and 0.5 by considering that to avoid distortions the minimum pulse width has to be $2\tau_g$. For the fast light, the maximum group delay is $\simeq 0.5\tau_g$. The gain-dispersion features can be altered by changing the values of the parameters, in particular by changing β. For comparison, we plot in Figs. 6(a) and 6(b) the group delay Δt_m for different orders m and for (a) $\beta=3$ and (b) $\beta=30$.

V. EXPERIMENTAL REALIZATION OF FAST AND SLOW LIGHTS

A. Experimental setup

The experimental setup is schematically represented in Fig. 7. Two-wave mixing is performed by interfering on the

LCLV a weak signal beam together with a higher intensity pump beam. The two beams originate from a cw solid state laser, $\lambda=532$ nm. They are enlarged and collimated; the beam diameter on the LCLV is 18 mm. The light polarization is linear and parallel to the LC nematic director. The intensity of the pump beam is fixed to $I_p=1.8$ mW/cm^2, whereas the signal beam is time modulated to obtain a Gaussian wave packet with a width larger than the LC response time. The signal pulse is shaped by using a spatial-light modulator. Its center frequency can be changed by a few hertz with a piezoelectrically driven mirror, its peak intensity I_s is kept much less than the pump intensity, and the ratio $\beta \equiv I_p/I_s$ being fixed to 30. The voltage applied to the LCLV is 20 V_{rms} at a frequency of 1 kHz.

When the two beams interfere in the plane of the photoconductor, they give rise to intensity fringes. In correspondence, the LC molecules reorient, thus inducing a phase grating in the LC layer, which acts as a dynamic hologram creating self-diffracted beams. The fringe spacing and, correspondingly, the period of the grating vary in between 50 and 300 μm, that is, larger than the LC thickness so that we deal with a thin grating and the beam coupling occurs in the Raman-Nath regime of diffraction with several output order beams.

Signal amplification originates from the self-diffraction of the pump, which transfers photons in the multiple directions due to the Raman-Nath regime. Depending on the frequency detuning δ between pump and signal, the m order output pulse can be amplified or attenuated. For each output order beam, we measure the gain as the ratio of the output intensity with respect to the input signal intensity I_s. For the parameters used in the experiment, the gain is >1 for $m=0$ and -2, the two orders symmetrical to the pump ($m=-1$), whereas is <1 for the other orders.

B. Experimental results

In Fig. 8 we show two representative experimental data, displaying (a) a fast-light pulse taken at the $m=0$ output and (b) a slow-light pulse at the $m=-2$ output. The input pulse widths were (a) 140 and (b) 180 ms, the grating spacings were (a) $\Lambda=110$ μm and (b) $\Lambda=300$ μm, and the frequency detunings were (a) $\delta/2\pi=3$ Hz and (b) $\delta=0$ Hz. For better visualization of the temporal shift, all the intensities are normalized to their peak value. In reality, the peak intensity of the fast-light pulse is 0.2 that of the input, while the slow-light pulse is amplified of a factor 2.2.

By fitting each pulse with a Gaussian, we have evaluated the time anticipation as $\Delta t_0=-65$ ms for the fast pulse and the time retardation as $\Delta t_{-2}=110$ ms for the slow pulse. The corresponding fractional delay is 0.58. The effective group velocity of each pulse can be determined as $v_m=d/\Delta t_m$. We obtain $v_0=-0.21$ mm/s for the fast pulse and $v_{-2}=0.13$ mm/s for the slow pulse.

For fixed parameters, $\Lambda=180$ μm, $\tau_{LC}=120$ ms, pulse width of 290 ms, and $\beta=30$, we plot in Fig. 9(a) the maximum group delay $\Delta t_m^{(max)}/\tau_{LC}$ measured for different order outputs. The experimental data (black dots) are reported together with the theoretical points (red dots). For the same

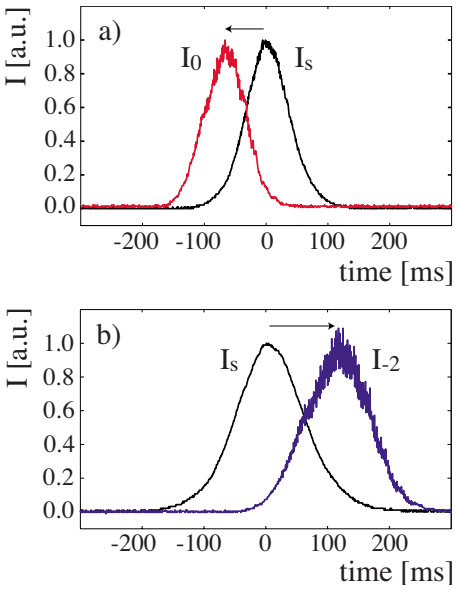

FIG. 8. (Color online) Experimental time dependencies of the output pulse taken on the (a) $m=0$ (red line) and (b) $m=-2$ (blue line) diffraction orders of the input pulse (black line). The time (a) anticipation and (b) delay are marked by the arrow.

values of parameters, we plot in Fig. 9(b) the group velocity of the pulse v_m versus the frequency detuning δ for $m=0$ and $m=-2$. A good agreement between the theoretical prediction and the experimental points is achieved. For $m=0$ we observe a second branch corresponding to fast light, whereas for $m=-2$ we have only the slow-light branch with a minimum group velocity of less than 0.2 mm/s. Such a small value of the group velocity corresponds to a very large group index, on the order of 10^{12}, which could be very attractive

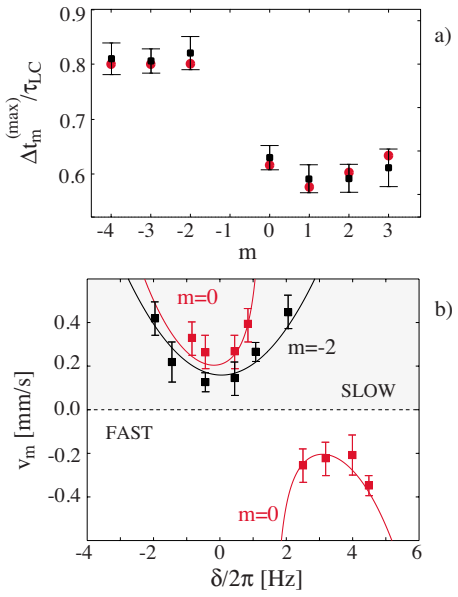

FIG. 9. (Color online) (a) Maximum group delay $\Delta t_m^{(max)}$ vs the order m of the output order; red dots are numerical points and black squares are experimental data; $\tau_{LC}=120$ ms and $\delta=0$. (b) Group velocity v_g vs $\delta/2\pi$ for $m=0$ (red) and $m=-2$ (black); lines are theoretical and squares are experimental points.

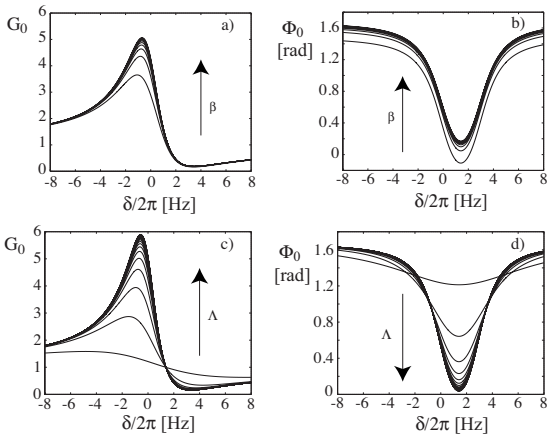

FIG. 10. Gain and phase shift for the $m=0$ output order beam calculated for [(a) and (b)] different values of β and $\Lambda=250$ μm and [(c) and (d)] different values of Λ and $\beta=80$.

for applications in ultrahigh precision interferometry.

VI. TUNING THE GROUP VELOCITY

The group velocity can be tuned by changing the experimental parameters. Here, we will focus in particular on the behavior of the order outputs $m=0$, $+1$, and -2 since they are of most practical use in the experiments. However, similar behaviors can be obtained also for the other higher order output pulses. In Fig. 10 we show the dependence of the gain G_0 and phase shift Φ_0 on the parameter β and on the spacing Λ of the refractive index grating. Both β and Λ are increased by steps of 10, β changes from 10 to 1000, and Λ changes from 50 to 1000 μm. The other parameters are fixed to $\tau_{LC}=120$ ms, $l_d=14$ μm, and $n_2=-6$ cm^2/W. We see that for increasing β or Λ all curves cumulate on a common profile.

Similar behaviors are obtained for the $m=+1$ and $m=-2$ orders. These are shown in Figs. 11 and 12, respectively. In these plots both β and Λ are increased by steps of 10, β changes from 20 to 1000, and Λ changes from 50 to 1000 μm. The other parameters are the same as for Fig. 10.

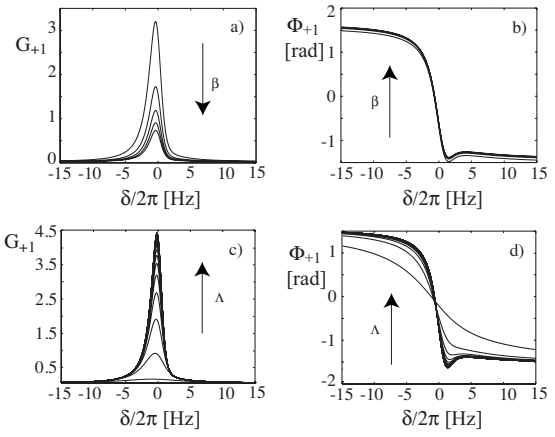

FIG. 11. Gain and phase shift for the $m=+1$ output order beam calculated for [(a) and (b)] different values of β and $\Lambda=250$ μm and [(c) and (d)] different values of Λ and $\beta=80$.

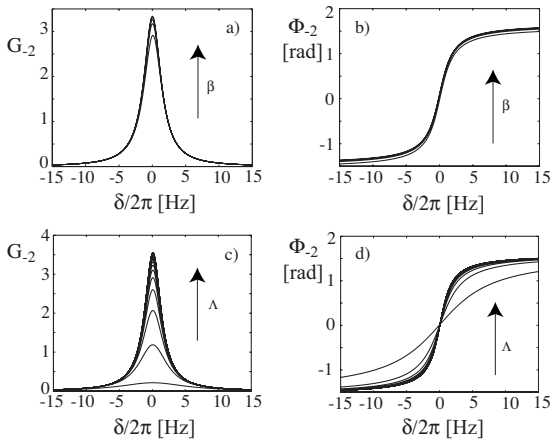

FIG. 12. Gain and phase shift for the $m=-2$ output order beam calculated for [(a) and (b)] different values of β and $\Lambda=250$ μm and [(c) and (d)] different values of Λ and $\beta=80$.

The group velocity changes accordingly with the behavior of the phase curves. For the $m=0$ output order we have calculated the dependence of the group delay on the pump intensity I_p and on the nonlinear coefficient n_2. Note that this last one can be changed in the experiment by varying the voltage V_0 applied to the LCLV, as shown in Fig. 4. The calculated group delay Δt_0 is plotted together with the experimental points as a function of I_p in Fig. 13 and as a function of n_2 in Fig. 14. Two different values of β, $\beta=3$ and 30, have been used while the other parameters have been kept fixed to $\Lambda=250$ μm, $\tau_{LC}=120$ ms, and $l_d=14$ μm. In Fig. 13 the value of the nonlinear coefficient is $n_2=-6$ cm^2/W, while in Fig. 14 the pump intensity is fixed to $I_p=1.5$ mW/cm^2.

We can see that increasing β allows to get a larger region of I_p for a fine tuning of Δt_0. On the other side, for small β the curve is nonmonotonic, so that Δt_0 can either be increased or decreased when increasing the pump intensity. As for the dependence on n_2, the curves are monotonic for all values of β. Correspondingly, the group velocity can be finely tuned by changing the voltage V_0 applied to the LCLV. The experimental measurements are in good agreement with the theoretical curves.

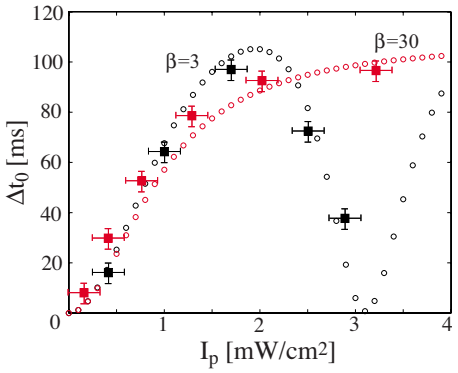

FIG. 13. (Color online) Group delay Δt_0 vs the pump intensity; black dots $\beta=3$, red dots $\beta=30$; $n_2=-6$ cm^2/W. Black and red squares are experimental points measured for $\beta=3$ and 30, respectively.

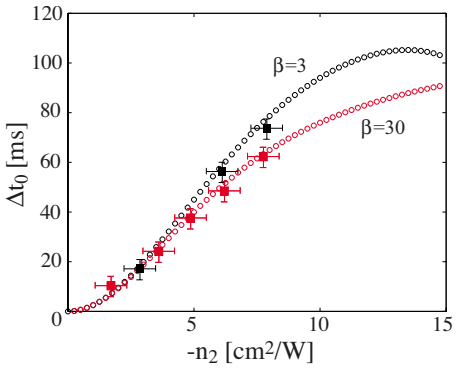

FIG. 14. (Color online) Group delay calculated Δt_0 vs the nonlinear coefficient n_2; black dots $\beta=3$ and red dots $\beta=30$; $I_p=1.5$ mW/cm^2. Black and red squares are experimental points measured for $\beta=3$ and 30, respectively.

VII. CONCLUSIONS AND PERSPECTIVES OF FURTHER DEVELOPMENTS

In conclusion, photorefractive LCLVs are attractive devices showing large and tunable nonlinear response and excellent photosensitivity coming from the association of the photoconductive layer with the large birefringence of the liquid crystals. Here, we have shown that by performing two-wave mixing experiments in LCLVs and by using the dispersive properties associated with the two-beam-coupling process, we can obtain fast- and slow-light phenomena with very large group delay. The corresponding group index, which is as large as 10^{12}, could be exploited to enhance the sensitivity of a slow-light interferometer. The group velocity can be finely tuned by changing the control parameters of the experiment, in particular by varying the strength of the nonlinearity. Experimentally, this is realized by changing the amplitude of the voltage applied to the LCLV.

During the wave mixing process the output pulse is amplified, thanks to the coupling with the pump beam, which transfers photons in the direction of the original signal. In the LCLV the process of optical amplification occurs in the Raman-Nath regime of diffraction and, since energy is scattered into several orders, this not as not as efficient as in the Bragg regime. However, the Raman-Nath diffraction scheme allows us to easily obtain signal multiplexing, with different replicas of the output beam occurring simultaneously and with different group delays. In particular, the dispersive properties of the $m=-2$ diffracted order are optimized for maximum slow light, allowing a larger group delay with respect to the group delay obtained in the Bragg regime. At the same time, fast light can easily be obtained on the $m=0$ order, with superluminal pulses that are only slightly depleted with respect to the original signal.

The working wavelength of the LCLV here presented ranges from 400 to 600 nm. In the future, extension to other spectral regions could be reached by the use of other types of photoconductive layers, such as doped photorefractive materials, semiconductors, or polymers.

The large group delay provided by the LCLV, which is a consequence of the highly dispersive properties of the wave mixing process, is indeed related to the slow response time needed to build up the grating inside the liquid-crystal layer. Such a slow response time is a limitation for certain applications, nevertheless, is well adapted for the detection of slow and very small deformations or displacements.

Moreover, for small positive detuning we have negative group delay on the $m=0$ order, while the same two-wave mixing process can be used to inject photons inside a cavity [34]. These two properties, fast-light associated with an optical resonator, could be exploited to increase the sensitivity of laser gyroscopes in the perspective of measuring absolute rotations with high precision [35].

Finally, the theoretical model here developed could be applied to any thin Kerr medium, provided it allows performing two-wave mixing experiments. Therefore, we expect that the slow- and fast-light schemes here proposed could be easily extended to other systems, such as thin photorefractive materials, dye-doped liquid crystals, and photorefractive polymers.

ACKNOWLEDGMENTS

This work has been partially supported by the Agence Nationale de la Recherche (Grant No. ANR-07-BLAN-0246-03 (*turbonde*).

[1] R. W. Boyd and D. J. Gauthier, in *Progress in Optics*, edited by E. Wolf (Elsevier Science, Amsterdam, 2002), Vol. 43, pp. 497–530.
[2] F. Xia, L. Sekaric, and Y. Vlasov, Nat. Photonics **1**, 65 (2007).
[3] Z. Shi, R. W. Boyd, D. J. Gauthier, and C. C. Dudley, Opt. Lett. **32**, 915 (2007); Z. Shi, R. W. Boyd, R. M. Camacho, Praveen Kumar Vudya Setu, and J. C. Howell, Phys. Rev. Lett. **99**, 240801 (2007).
[4] G. S. Pati, M. Salit, K. Salit, and M. S. Shahriar, Phys. Rev. Lett. **99**, 133601 (2007).
[5] H. N. Yum, M. Salit, G. S. Pati, S. Tseng, P. R. Hemmer, and M. S. Shahriar, Opt. Express **16**, 20448 (2008).
[6] A. Kasapi, M. Jain, G. Y. Yin, and S. E. Harris, Phys. Rev. Lett. **74**, 2447 (1995).
[7] L. V. Hau, S. E. Harris, Z. Dutton, and C. H. Behroozi, Nature (London) **397**, 594 (1999).
[8] M. S. Bigelow, N. N. Lepeshkin, and R. W. Boyd, Phys. Rev. Lett. **90**, 113903 (2003).
[9] E. Podivilov, B. Sturman, A. Shumelyuk, and S. Odoulov, Phys. Rev. Lett. **91**, 083902 (2003).
[10] A. Shumelyuk, K. Shcherbin, S. Odoulov, B. Sturman, E. Podivilov, and K. Buse, Phys. Rev. Lett. **93**, 243604 (2004).
[11] G. Zhang, R. Dong, F. Bo, and J. Xu, Appl. Opt. **43**, 1167 (2004); G. Zhang, F. Bo, R. Dong, and J. Xu, Phys. Rev. Lett. **93**, 133903 (2004).
[12] Q. Yang, J. T. Seo, B. Tabibi, and H. Wang, Phys. Rev. Lett.

95, 063902 (2005).
[13] S. Residori, U. Bortolozzo, and J. P. Huignard, Phys. Rev. Lett. **100**, 203603 (2008).
[14] R. M. Camacho, C. J. Broadbent, I. Ali-Khan, and J. C. Howell, Phys. Rev. Lett. **98**, 043902 (2007).
[15] P. Aubourg, J. P. Huignard, M. Hareng, and R. A. Mullen, Appl. Opt. **21**, 3706 (1982).
[16] U. Bortolozzo, S. Residori, and J. P. Huignard, J. Nonlinear Opt. Phys. Mater. **16**, 231 (2007).
[17] U. Bortolozzo, S. Residori, and J. P. Huignard, J. Phys. D **41**, 224007 (2008).
[18] A. Yariv, *Optical Waves in Crystals* (Wiley, New Jersey, 2003), pp. 354–358.
[19] P. Gunter and J. P. Huignard, *Photorefractive Materials and Their Applications 1* (Springer, New York, 2006).
[20] P. G. De Gennes and J. Prost, *The Physics of Liquid Crystals*, 2nd ed. (Clarendon, Oxford, 1993).
[21] J. Cognard, Mol. Cryst. Liq. Cryst. Suppl. Ser. **1**, 1 (1982).
[22] P. Yeh and C. Gu, *Optics of Liquid Crystal Displays* (Wiley, New York, 1990).
[23] D. Armitage, J. I. Thackara, and W. D. Eades, Appl. Opt. **28**, 4763 (1989).
[24] N. V. Kukhtarev, V. B. Markov, S. G. Odulov, M. S. Soskin, and V. L. Vinetskii, Ferroelectrics **22**, 949 (1979).
[25] J. P. Huignard and A. Marrakchi, Opt. Lett. **6**, 622 (1981).
[26] Ph. Dittrich, G. Montemezzani, P. Bernasconi, and P. Gunter, Opt. Lett. **24**, 1508 (1999).
[27] M. Segev, B. Crosignani, A. Yariv, and B. Fischer, Phys. Rev. Lett. **68**, 923 (1992).
[28] J. L. de Bougrenet de la Tocnaye, P. Pellat-Finet, and J. P. Huignard, J. Opt. Soc. Am. B **3**, 315 (1986).
[29] F. T. Arecchi, G. Giacomelli, P. L. Ramazza, and S. Residori, Phys. Rev. Lett. **65**, 2531 (1990).
[30] U. Bortolozzo, P. Villoresi, and P. L. Ramazza, Phys. Rev. Lett. **87**, 274102 (2001).
[31] U. Bortolozzo, S. Residori, and J. P. Huignard, Opt. Lett. **31**, 2166 (2006).
[32] H. Kogelnik, Bell Syst. Tech. J. **48**, 2909 (1969).
[33] A. Brignon, I. Bongrand, B. Loiseaux, and J. P. Huignard, Opt. Lett. **22**, 1855 (1997).
[34] U. Bortolozzo, A. Montina, F. T. Arecchi, J. P. Huignard, and S. Residori, Phys. Rev. Lett. **99**, 023901 (2007).
[35] M. S. Shahriar, G. S. Pati, R. Tripathi, V. Gopal, M. Messall, and K. Salit, Phys. Rev. A **75**, 053807 (2007).